Unsupported Ti−Co and Zr−Co Bonds in Heterobimetallic Complexes: A Theoretical Description of Metal−Metal Bond Polarity

Georg Jansen,*,† Martin Schubart,‡ Bernd Findeis,‡ Lutz H. Gade,*,‡ Ian J. Scowen,§ and Mary McPartlin§

Contribution from the Institut für Theoretische Chemie der Universität Düsseldorf, Universitätsstrasse 1, 40225 Düsseldorf, Germany, Institut für Anorganische Chemie der Universität Würzburg, Am Hubland, 97074 Würzburg, Germany, and School of Applied Chemistry, University of North London, Holloway Road, London N7 8DB, U.K.

Received December 8, 1997

Abstract: The synthesis, structural, and theoretical characterization of heterobimetallic complexes $[CH_3Si\{SiMe_2N(4\text{-}CH_3C_6H_4)\}_3M-Co(CO)_3(L)]$ (M = Ti, Zr; L = CO, PPh_3, $PTol_3$) with unsupported metal−metal bonds between cobalt atoms and titanium or zirconium atoms is being reported. The synthesis of the dinuclear compounds was achieved by salt metathesis of the chlorotitanium and zirconium complexes and the alkalimetal carbonylates. X-ray crystal structure analyses of four of these heterobimetallic complexes established the unsupported metal−metal bonds [M = Ti, L = CO (**3**): 2.554(1) Å; M = Ti, L = $PTol_3$ (**4b**): 2.473(4) Å; M = Zr, L = CO (**5**): 2.705(1) Å; M = Zr, L = PPh_3 (**6a**): 2.617(1) Å] as well as the 3-fold molecular symmetries. Upon axial phosphine substitution, a metal−metal bond contraction of ca. 0.08 Å is observed, which also results in the quantum chemical structure optimizations performed on the model compounds $[(H_2N)_3Ti-Co(CO)_4]$ (**3x**) and $[(H_2N)_3Ti-Co(CO)_3(PH_3)]$ (**4x**) using gradient-corrected and hybrid density functionals. A theoretical study of the homolytic dissociation of the metal−metal bonds focuses on the relaxation energies of the complex fragments and indicates that the geometrical constraints imposed by the tripod ligand lead to a major thermodynamic contribution to the stability of the experimentally investigated complexes. The central question of the polarity of the metal−metal bond is addressed by detailed analysis of the calculated electron charge distribution using natural population analysis (NPA), charge decomposition analysis (CDA), Bader's atoms in molecules (AIM) theory, and the electron localization function (ELF). Both the orbital-based NPA and CDA schemes and the essentially orbital-independent AIM and ELF analysis suggest a description of the Ti−Co bond as being a highly polar covalent single bond. The combination of AIM and ELF is employed for the first time to analyze metal−metal bond polarity and appears to be a powerful theoretical tool for the description of bond polarity in potentially ambiguous situations.

Heterobimetallic complexes involving the metals of the Ti-triad and late transition metals joined by an unsupported metal−metal bond have been studied for more than a decade.[1] A theoretical analysis of such metal−metal bonding was first provided by Bursten and Novo-Gradac, who applied Xα-SW molecular orbital methods to the system $Cp_2(X)Zr-Ru(CO)_2Cp$.[2] Shortly thereafter, Wolczanski and co-workers published extended Hückel MO calculations on various early−late heterobimetallic complexes.[3] Both studies offered a qualitative analysis of the principal bonding interactions between the early and the late metal centers. Recently, Selent et al. reported the results of an EHMO study of $(t\text{BuO})_3Ti\text{-}M(CO)_n$ (M = Co/Mn, $n = 4/5$).[4] However, the published theoretical analyses of the M−M′ bonds, based on the metric parameters derived from various crystal structures although providing some valuable insight into the nature of this class of compounds, are unsuitable for addressing such questions as metal−metal bond polarity in even a semiquantitative way.

The concept of bond polarity, which is used in main group chemistry with reference to the electronegativities of the atoms involved, is less readily applied in a quantitative way to bonds between transition metals. Their nature may be more significantly influenced by the coordination spheres of the two or more metal centers involved rather than intrinsic properties of the metal itself. This increased level of sophistication required in a meaningful discussion of bond polarity in M−M′ bonds necessitates elaborate quantum chemical methods to be used. However, this may render it difficult to extract information from the results of such calculations that are interpretable within the established paradigms of structure and bonding familiar to the chemist.

† Universität Düsseldorf.
‡ Universität Würzburg.
§ University of North London.

(1) (a) Casey, C. P.; Jordan, R. F.; Rheingold, A. L. *J. Am. Chem. Soc.* **1983**, *105*, 665. (b) Casey, C. P.; Jordan, R. F.; Rheingold, A. L. *Organometallics* **1984**, *3*, 504. (c) Sartain, W. S.; Selegue, J. P. *J. Am. Chem. Soc.* **1985**, *107*, 5818. (d) Sartain, W. S.; Selegue, J. P. *Organometallics* **1987**, *6*, 1812. (e) Sartain, W. S.; Selegue, J. P. *Organometallics* **1989**, *8*, 2153. (f) Casey, C. P. *J. Organomet. Chem.* **1990**, *400*, 205. (g) Selent, D.; Beckhaus, R.; Pickardt, J. *Organometallics* **1993**, *12*, 2857. (h) Friedrich, S.; Gade, L. H.; Scowen, I. J.; McPartlin, M. *Organometallics* **1995**, *14*, 5344. (i) Friedrich, S.; Gade, L. H.; Scowen, I. J.; McPartlin, M. *Angew. Chem., Int. Ed. Engl.* **1996**, *35*, 1338.

(2) (a) Bursten, B. E.; Novo-Gradac, K. J. *J. Am. Chem. Soc.* **1987**, *109*, 904. (b) Bursten, B. E.; Strittmatter, R. J. *Angew. Chem., Int. Ed. Engl.* **1991**, *30*, 1069.

(3) Ferguson, G. S.; Wolczanski, P. T.; Parkanyi, L.; Zonnevylle, M. *Organometallics* **1988**, *7*, 1967.

(4) Selent, D.; Ramm, M.; Janiak, C. *J. Organomet. Chem.* **1995**, *501*, 235.

S0002-7863(97)04160-7 CCC: $15.00
Published on Web 07/10/1998

It was our aim to investigate to which extent modern DFT methods are suitable for a detailed theoretical investigation of such systems, in particular whether metric parameters obtained for adequate models of real systems are able to emulate those obtained experimentally by X-ray crystallography. We note that Ziegler and co-workers first performed DFT calculations on metal−metal-bonded complexes more than a decade ago,[5,6] although the local spin density approximation codes available at that time set the limit to the accuracy with which the metric parameters could be calculated. Very Recently, Cotton and Feng have demonstrated in their theoretical study of several metal−metal multiply bonded dinuclear complexes that modern gradient-corrected DFT methods, which yielded structural data in excellent agreement with the experimental results, may be a powerful predictive tool in this field of inorganic chemistry.[7]

A second aim of this work was to establish the polarity of the bond between the different metal centers by careful analysis of the charge distributions obtained by the DFT methods. To this end, several independent theoretical approaches were employed. On one hand, orbital-based population analysis schemes such as natural population analysis (NPA)[8] in combination with Wiberg bond indices[9] and carge decomposition analysis (CDA)[10] were employed. On the other hand, essentially orbital independent methods such as Bader's AIM (atoms in molecules) approach[11−13] in combination with Becke's, Edgecombe's, and Savin's ELF (electron localization function)[14,15] were employed. As will be shown below, we feel that an unambiguous assignment of metal−metal bond polarity can be made on the basis of a combination of AIM and ELF and that the emerging picture is in accord with that suggested by the more traditional population analyses, but much less dependent upon the technicalities of the calculations such as the choice of the basis functions.

The Objects of Study

An important aspect governing the choice of an appropriate system of study was the molecular symmetry of the heterodinuclear complex. To facilitate the interpretation of the results obtained in calculations and in the experimental structural studies, both complex fragments joined through the direct metal−metal (M−M′) bond should have the same symmetry with respect to this bonding axis. The use of tripodal amido ligands for the stabilization of the tetravalent early transition metal fragment therefore essentially dictated their combination with a late transition metal fragment of the type $\{M'(L)_3L'\}$ (L′ occupying a *trans*-axial position with respect to the M−M′ bond). The most readily available such species are derived from the monoanions $[Co(CO)_3(L)]^-$ (L = CO, PR_3).

We have previously shown that Ti−Co heterobimetallic complexes of the types $RC(CH_2NSiMe_3)_3Ti-Co(CO)_3(PR'_3)$ and $HC(SiMe_2NTol)_3Ti-Co(CO)_3(PR'_3)$ (R = CH_3, C_6H_5; R′ = C_6H_5, 4-$CH_3C_6H_4$; Tol = 4-$CH_3C_6H_4$) may be sufficiently stable to be fully characterized analytically and specroscopically.[16,17] The availability of a tripodal amido ligand system suitable for coordination to both first row as well as second and third row transition metals[18] prompted us to systematically probe the influence that the combination of the metals as well as the *trans*-axial ligand at the Co center have on the structural parameters associated with the M−Co bond.

In this paper, we report the synthesis of Ti−Co and Zr−Co heterodinuclear complexes in which the *trans*-axial position at the Co atom is occupied either by a CO or a triarylphosphine ligand. An X-ray crystallographic study of four compounds containing Ti−Co and Zr−Co bonds, with and without *trans*-axial phosphine substitution, provides the experimental "point of reference" for the metric parameters that characterize these complexes. On the basis of these structures, a model Ti−Co system is discussed upon which the theoretical work was performed.

Synthesis and Crystal Structures of Ti−Co and Zr−Co Heterobimetallic Complexes

The tripodal amido complexes $MeSi\{SiMe_2N(4\text{-}CH_3C_6H_4)\}_3$-MX (M = Ti, X = Br: **1**; M = Zr, X = Cl: **2**) were the early transition metal building blocks for the synthesis of the early−late heterobimetallic compounds. The unsupported metal−metal bonds were formed by salt metathesis of the halide complexes with $Na[Co(CO)_3(L)]$ (L = CO, PPh_3, $PTol_3$) under analogous reaction conditions to those previously employed in the synthesis of Ti−M and Zr−M complexes (M = Fe, Ru).[16,19,20] Although monitoring the reactions by ^{1}H NMR spectroscopy indicated almost quantitative conversions to the desired heterodinuclear compounds **3**−**6** (Scheme 1), the isolated yields were moderate (37−73%) due to losses upon crystallization from the reaction mixtures.

A qualitative analysis of highly polar metal−metal bonding in Co−Ga heterobimetallics has been attempted by Fischer et al. on the basis of the (CO) wavenumbers in analogy to previous assignments of complexes containing $CpM(CO)_2$ fragments.[21] Whereas for the latter a consistent qualitative picture has emerged both for the group 8−13 as well as the group 4−8 heterobimetallics investigated by us and others, the carbonyl frequencies in the cobalt complexes are scattered over a fairly

(5) (a) Ziegler, T. *J. Am. Chem. Soc.* **1983**, *105*, 7543. (b) Ziegler, T. *J. Am. Chem. Soc*. **1984**, *106*, 5901. (c) Ziegler, T. *J. Am. Chem. Soc*. **1985**, *107*, 4453. (d) Ziegler, T. *Chem. Rev*. **1991**, *91*, 651.

(6) More recent applications of modern DFT methods: (a) Ziegler, T.; Tschinke, V.; Becke, A. *Polyhedron* **1987**, *6*, 685. (b) Folga, E.; Ziegler, T. *J. Am. Chem. Soc*. **1993**, *115*, 5169. (c) Rosa, A.; Ricciardi, G.; Baerends, E. J.; Stufkens, D. J. *Inorg. Chem*. **1995**, *34*, 3425. (d) Provencher, R.; Harvey, P. D. *Inorg. Chem*. **1996**, *35*, 2113. (e) Lovell, T.; McGrady, J. E.; Stranger, R.; Macgregor, S. A. *Inorg. Chem*. **1996**, *35*, 3079. (f) Bo, C.; Costas, M.; Poblet, J. M.; Rohmer, M. M.; Benard, M. *Inorg. Chem*. **1996**, *35*, 3298. (g) Jacobsen, H.; Ziegler, T. *J. Am. Chem. Soc*. **1996**, *118*, 4631. (h) Rosa, A.; Ehlers, A. W.; Baerends, E. J.; Snijders, J. G.; te Velde, G. *J. Phys. Chem*. **1996**, *100*, 5690.

(7) Cotton, F. A.; Feng, X. *J. Am. Chem. Soc*. **1997**, *119*, 7514.

(8) Reed, A. E.; Curtiss, L. A.; Weinhold, F. *Chem. Rev*. **1988**, *88*, 899.

(9) Wiberg, K. A. *Tetrahedron* **1968**, *24*, 1083.

(10) Dapprich, S.; Frenking, G. *J. Phys. Chem*. **1995**, *99*, 9352.

(11) Bader, R. F. W. *Atoms in Molecules*: *A Quantum Theory*; Oxford University Press: Oxford, 1990.

(12) (a) Bader, R. F. W.; Popelier, P. L. A.; Keith, T. A. *Angew. Chem., Int. Ed. Engl*. **1994**, *33*, 620.

(13) (a) Bader, R. F. W. *Chem. Rev*. **1991**, *91*, 893. (b) Bader, R. F. W.; Nguyen-Dank, T. T.; Tal, Y. *Rep. Prog. Phys*. **1981**, *44*, 893.

(14) Becke, A. D.; Edgecombe, K. E. *J. Chem. Phys*. **1990**, *92*, 5397.

(15) Savin, A.; Nesper, R.; Wengert, S.; Fässler, T. F. *Angew. Chem., Int. Ed. Engl*. **1997**, *36*, 1808.

(16) Friedrich, S.; Memmler, H.; Gade, L. H.; Li, W.-S.; McPartlin, M. *Angew. Chem., Int. Ed. Engl*. **1994**, *33*, 676.

(17) Friedrich, S.; Memmler, H.; Gade, L. H.; Li, W.-S.; McPartlin, M.; Housecroft, C. E. *Inorg. Chem*. **1996**, *35*, 2433.

(18) (a) Gade, L. H.; Mahr, N. *J. Chem. Soc., Dalton Trans*. **1993**, 489. (b) Hellmann, K. W.; Gade, L. H.; Li, W.-S.; McPartlin, M. *Inorg. Chem*. **1994**, *33*, 5974. (c) Gade, L. H.; Becker, C.; Lauher, J. W. *Inorg. Chem*. **1993**, *32*, 2308. (d) Friedrich, S.; Gade, L. H.; Edwards, A. J.; McPartlin, M. *Chem. Ber*. **1993**, *126*, 1797. (e) Memmler, H.; Gade, L. H.; Lauher, J. W. *Inorg. Chem*. **1994**, *33*, 3064. (f) Schubart, M.; Findeis, B.; Gade, L. H.; Li, W.-S.; McPartlin, M. *Chem. Ber*. **1995**, *128*, 329.

(19) Findeis, B.; Schubart, M.; Platzek, C.; Gade, L. H.; Scowen, I. J.; McPartlin, M. *Chem. Commun*. **1996**, 219.

(20) Friedrich, S.; Gade, L. H.; Scowen, I. J.; McPartlin, M. *Angew. Chem., Int. Ed. Engl*. **1996**, *35*, 1338.

(21) Fischer, R. A.; Miehr, A.; Priermeier, T. *Chem. Ber*. **1995**, *128*, 831.

Scheme 1. Synthesis of the M−Co−Heterobimetallics (M = Ti, Zr)

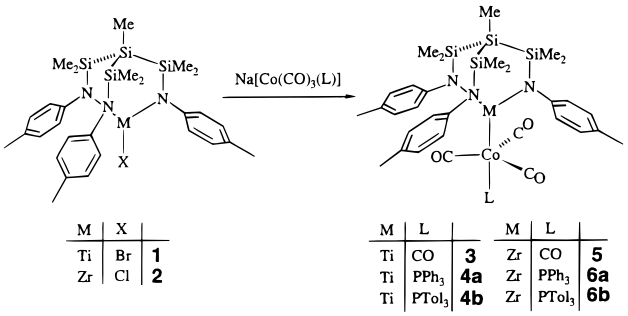

M	X	
Ti	Br	**1**
Zr	Cl	**2**

M	L	
Ti	CO	**3**
Ti	PPh_3	**4a**
Ti	$PTol_3$	**4b**

M	L	
Zr	CO	**5**
Zr	PPh_3	**6a**
Zr	$PTol_3$	**6b**

Table 1. Principal Bond Lengths and Angles for Compounds **3** and **4b** (M = Ti) and **5** and **6a** (M = Zr)

	3	**4b**	**5**	**6a**
M−Co	2.5542(10)	2.471(4)	2.7051(11)	2.6175(14)
M−N(1)	1.923(3)	1.923(10)	2.037(5)	2.056(4)
M−N(2)	1.916(3)		2.044(5)	
M−N(3)	1.926(3)		2.032(5)	
Co−C(41)	1.756(6)	1.771(11)	1.762(8)	1.748(6)
Co−C(42)	1.758(6)		1.762(8)	
Co−C(43)	1.774(6)		1.765(8)	
Co−C(44)	1.784(6)		1.788(8)	
Co−P(1)		2.238(5)		2.217(3)
O(1)−C(41)	1.154(6)	1.151(13)	1.150(7)	1.155(6)
O(2)−C(42)	1.155(6)		1.144(7)	
O(3)−C(43)	1.141(5)		1.148(8)	
O(4)−C(44)	1.156(6)		1.142(8)	
M−Co−C(41)	83.5(2)	85.0(4)	80.3(2)	84.3(2)
M−Co−C(42)	81.0(2)		80.4(2)	
M−Co−C(43)	82.1(2)		81.5(2)	
M−Co−C(44)	176.9(2)		178.0(3)	
M−Co−P(1)		180.0		180.0

wide range that make an assessment of the actual bond polarity extremely difficult. However, the Co−Ga and Co−Al compound have been studied theoretically in some detail by Frenking and co-workers, who concluded that the metal−metal bonds should be regarded as essentially pure donor−acceptor bonds,[22] a notion that is in accord with the tendency of these species to dissociate heterolytically in polar solvents such as thf and acetonitrile. In contrast, none of the Ti−Co and Zr−Co heterobimetallics reported in this paper were found to undergo appreciable ionic dissociation in either thf or CH_3CN (detectable by IR spectroscopy or conductivity measurements).

Single-crystal X-ray structure analyses were carried out for the Ti−Co species **3** and **4b** and the Zr−Co species **5** and **6a**, and the principal bond lengths and angles for the structures are given in Table 1. The phosphine-substituted complexes, **4b** and **6a**, each display crystallographic 3-fold symmetry with the phosphine phosphorus atom, the metal atoms, and the methylsilane apex of the tris-amido tripod aligned along the crystallographic C_3-axis (Figure 1). A similar 3-fold symmetric molecular structure exists in the tetracarbonylcobalt-derived species, **3** and **5**, although the crystallographic symmetry is disrupted in these cases.

In each complex, the trisilylsilane tripodal ligand framework as well as the N-bonded peripheral tolyl groups effectively shield the major part of the coordination sphere of the tetravalent metal center and generate a binding "pocket" in which the cobalt complex fragment is accommodated. The dimensions of this conical pocket appear to be dictated by the interplay of two factors.

(22) Boehme, C.; Frenking, G. *Book of abstracts of the 33rd Symposium für Theoretische Chemie*, September 21−25, 1997, Bornheim-Walberberg, Germany.

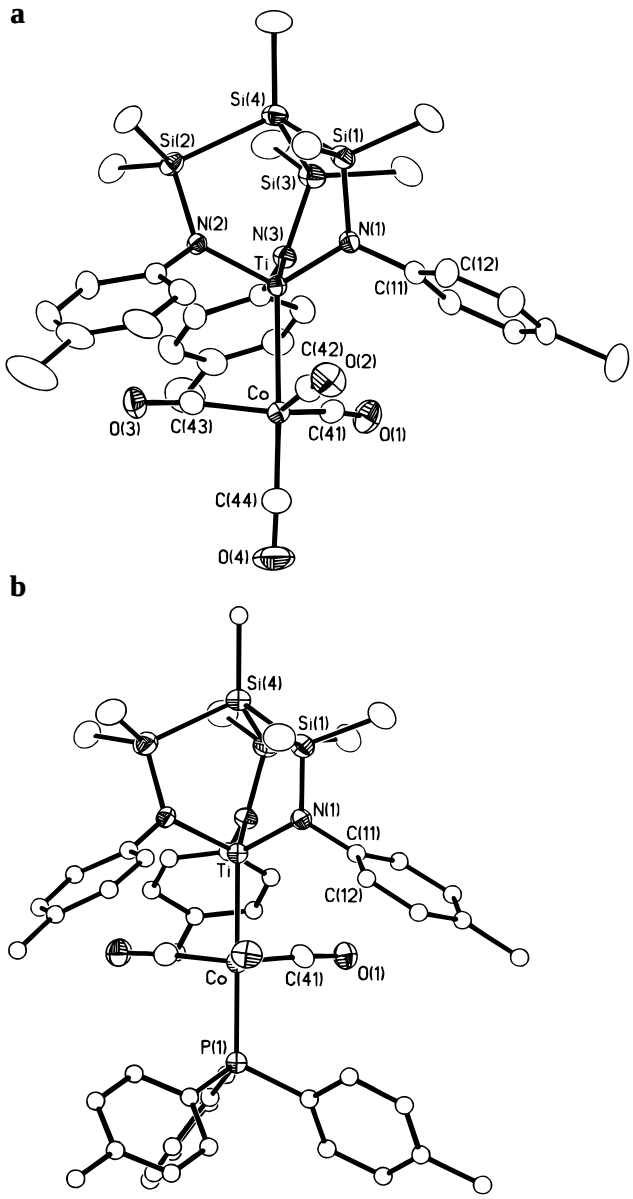

Figure 1. Molecular structures of **3** (a) and **4b** (b) viewed perpendicular to the Ti−Co bond axis. The molecular structures of the corresponding zirconium−cobalt compounds **5** and **6** are essentially identical. Thermal ellipsoids are shown with 20% probability.

The tripodal amido ligand in each complex shows a helical twist that may be envisaged as a rotation of the N_3 triangle of the ligand with respect to an Si_3 triangle described by the $SiMe_2$ units of each tripod arm (Figure 2); the torsion angles Si−Si−N-M that provide a measure for the extent of this twist lie in the range 11.2−31.4° with **6a** and **3** representing the lower and upper limits, respectively. This helical twisting of the tripod appears to arise both from steric repulsions of the methyl groups in the $SiMe_2$ units and, significantly, to alleviate the mismatch in dimensions of the trisilylsilane unit [d_{av}(Si−Si) = 2.340 Å] and the N_3M fragment [d_{av}(Ti−N) = 1.93, d_{av}(Zr−N) = 2.08 Å] within the metal tripod cage. It is notable that within comparable pairs of complexes (**3** and **6**, **4b** and **6a**) the smaller metal atom (Ti) induces the greatest twisting. Such twisting dictates the degree to which the tolyl groups are tilted toward the Co complex fragments. The theoretical study of model compounds closely related to **3** and **4b**, which is presented below, suggests that there may also be an electronic reason for the observed twist in the tripod cage.

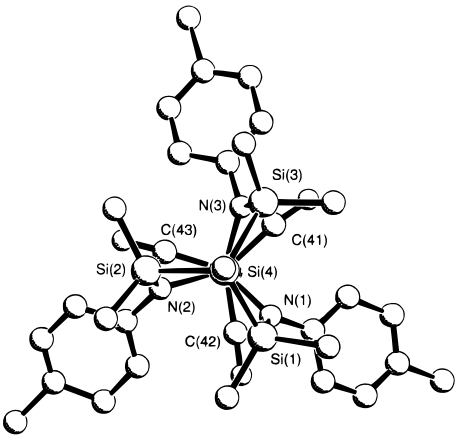

Figure 2. Molecular structure of **3** viewed along the molecular 3-fold axis to illustrate the twist within the tripod ligand coordinated to the early transition metal.

The second factor that controls the dimensions of the binding site for the late transition metal complex fragment involves the rotation of the tolyl groups about the N−C bond. Torsion angles with respect to the Si−N vectors [e.g., Si(1)−N(1)−C(11)−C(12)] lie in two distinct ranges: 57.3−62.3° for the tetracarbonylcobaltate derivatives and 82.8−90.8° for the phosphine-substituted species. It is noticeable, however, that within each pair of complexes the tolyl groups lie closer to a perpendicular disposition with respect to the "tripod arm" in the Zr species, which is commensurate with the smaller helical twist of the tripod cage. The interplay of these factors—that the most twisted ligands also feature the greater rotation of the tolyl periphery—appears therefore to promote the opening of the conical pocket for the cobalt complex fragment.

In each complex the cobalt fragment "locks" into the binding pocket of the tetravalent metal fragment so that the trigonal $Co(CO)_3$ unit is approximately staggered with respect to the N_3M unit. There appears to be little interaction between the carbonyls and the tolyl groups of the tris-amido ligand, the closest approaches being beyond 3 Å. Similarly, the aryl groups of the phosphine ligands show no significant interaction with the tolyl periphery of the tripod ligand—centroid−centroid distances of ca. 5.5 Å and interplanar angles of ca. 60° preclude significant $\pi-\pi$ interaction.[23]

The Ti−Co bond length of **3** [2.554(1) Å] is very close to that previously determined for $(t\text{BuO})_3\text{TiCo(CO)}_4$ [2.565(2) Å][1g] but significantly shorter than the metal−metal distance in the sterically crowded $[(CO)_9Co_3CO]_2CpTi-Co(CO)_4$ [2.614 Å].[24] Upon trans-axial phosphine substitution in **4b** the Ti−Co bond length is reduced to 2.473(4) Å, which therefore marks the lower limit to date. The Zr−Co bonds in **5** [d(Zr−Co) = 2.705(1) Å] and **6a** [d(Zr−Co) = 2.617(1) Å] are the first to be established by X-ray crystallography. In the four crystal structures, the equatorial CO ligands of the trigonal bipyramidally configurated Co fragment are bent toward the early transition metal centers [<(M−Co−CO) = 80.7(2)−85.3(4)°] (M = Ti, Zr); however, the distances between the carbonyl C atoms and the Ti(Zr) atoms are above 2.9 Å in all structures, thus precluding any semibridging interactions. In other words, the metal−metal bonds in these heterobimetallic complexes may be viewed as truly unsupported.

The most remarkable result of the crystal structure analyses of all four compounds is the contraction of the metal−metal bond upon substitution of the transaxial σ-donor/π-acceptor ligand CO by the better donor ligand triarylphosphine: Δd(Ti−Co) = 0.081 Å, Δd(Zr−Co) = 0.088 Å. A closer inspection of this contraction and its consequences for the charge distribution between the metals will be an important aspect of the theoretical study presented below.

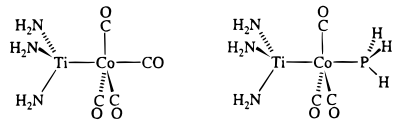

Figure 3. Model compounds **3x** and **4x** investigated in the theoretical study.

The Model Systems for Ti−Co Bonding

To reduce the complexity of the system in the theoretical study which follows, we chose to strip it of its chemical periphery. The model systems studied were thus the heterobimetallic complexes $(H_2N)_3Ti-Co(CO)_4$ (**3x**) and $(H_2N)_3Ti-Co(CO)_3(PH_3)$ (**4x**) (Figure 3).

While the peripheral substituents, particularly at the amido-N atoms, influence the stability of the real systems as well as (to a lesser extent) the electronic situation at the early transition metal center, the overall effects related to the metal−metal bonding are expected to be essentially unaltered. The experimentally determined average structural parameters were used as initial values in the full structural optimizations of the models, although the structures corresponding to the potential energy minima *were expected to differ* somewhat from those of **3** and **4b**. The conclusions drawn with respect to the bonding situation thus refer to the models **3x** and **4x** in the first place. A generalization that includes the "real" systems will be attempted.

The Calculated Structures of $(H_2N)_3Ti-Co(CO)_4$ and $(H_2N)_3Ti-Co(CO)_3(PH_3)$ and Their Comparison with Those of 3 and 4b

Two different exchange−correlation potentials were employed in the DFT calculations on the model systems: The BLYP combination of Becke's gradient correction to Slater exchange with the Lee−Yang−Parr correlation potential,[25] and the B3LYP combination with Becke's three-parameter hybrid functional.[26] Table 2 summarizes the principal structural parameters obtained from geometry optimizations of **3x** and **4x** (Figure 4) using the triple ζ-valence double polarization (TZVDP) basis set described in the section on computational methods (vide infra).

The bond lengths obtained with the BLYP functional are all greater than those obtained with the B3LYP functional. While the deviations are less than 0.01 Å for N−H and P−H bonds, they can become as large as 0.035 Å for the Co−Ti and Co−P bonds, with deviations in the range of 0.015−0.2 Å for the other bonds. This is in agreement with corresponding results of a recent study on transition metal compounds containing homonuclear metal−metal bonds.[7] Angles calculated with both functionals agree within about 0.5°, with the exception of the H(19)−P(18)−Co(1)−C(12) dihedral angle, which is computed to be −59.3° with the BLYP functional as compared to −46.4° with the B3LYP functional. This deviation, however, is practically irrelevant, as can be seen from the extremely small value of less than 0.2 kcal/mol determined for the barrier of rotation of the PH_3 group around the Co−P axis.

(23) Dance, I.; Scudder, M. *Chem. Eur. J.* **1996**, *2*, 481.
(24) Schmid, G.; Stutte, B.; Boese, R. *Chem. Ber.* **1978**, *111*, 1239.
(25) (a) Becke, A. D. *Phys. Rev. A* **1988**, *38*, 3098. (b) Lee, C.; Yang, W.; Parr, R. G. *Phys. Rev. B* **1988**, *37*, 785. (c) Miehlich, B.; Savin, A.; Stoll, H.; Preuss, H. *Chem. Phys. Lett.* **1989**, *157*, 200.
(26) (a) Becke, A. D. *J. Chem. Phys.* **1993**, *98*, 5648. (b) Barone, V. *Chem. Phys. Lett.* **1994**, *226*, 392.

Table 2. Calculated Structural Parameters for **3x** and **4x** and the Corresponding Parameters in the Experimentally Determined Structures of **3**[a] and **4b**

	3x				**4x**		
	BLYP	B3LYP	exptl. (**3**)		BLYP	B3LYP	exptl. (**4**)
			Distances (Å)				
Co(1)−Ti(2)	2.627	2.592	2.554	Co(1)−Ti(2)	2.558	2.529	2.471
Ti(2)−N(3)	1.908	1.889	1.922	Ti(2)−N(3)	1.913	1.894	1.923
N(3)−H(4)	1.023	1.015		N(3)−H(4)	1.023	1.014	
N(3)−H(5)	1.020	1.012		N(3)−H(5)	1.020	1.012	
Co(1)−C(12)	1.807	1.790	1.763	Co(1)−C(12)	1.796	1.780	1.771
C(12)−O(13)	1.163	1.148	1.150	C(12)−O(13)	1.168	1.152	1.151
Co(1)−C(18)	1.828	1.812	1.784	Co(1)−P(18)	2.258	2.225	2.238
C(18)−O(19)	1.156	1.141	1.156	P(18)−H(19)	1.422	1.412	
			Angles (deg)				
Co(1)−Ti(2)−N(3)	111.8	111.4	113.9	Co(1)−Ti(2)−N(3)	112.2	111.8	114.1
Co(1)−C(12)−O(13)	176.8	176.9	173.4	Co(1)−C(12)−O(13)	178.4	177.8	176.0
Ti(2)−N(3)−H(4)	123.5	123.8		Ti(2)−N(3)−H(4)	123.7	123.9	
Ti(2)−N(3)−H(5)	126.2	125.8		Ti(2)−N(3)−H(5)	125.9	125.5	
H(4)−N(3)−H(5)	110.0	110.3		H(4)−N(3)−H(5)	110.1	110.3	
N(3)−Ti(2)−N(6)	107.0	107.5	104.6	N(3)−Ti(2)−N(6)	106.6	107.1	104.5
Ti(2)−Co(1)−C(12)	79.4	79.7	82.2	Ti(2)−Co(1)−C(12)	81.7	81.8	85.0
C(12)−Co(1)−C(14)	116.7	116.9	118.2	C(12)−Co(1)−C(14)	118.0	118.0	119.3
C(12)−Co(1)−C(18)	100.6	100.3	97.8	C(12)−Co(1)−P(18)	98.3	98.2	95.0
				Co(1)−P(18)−H(19)	120.4	120.2	
				H(19)−P(18)−H(20)	96.7	97.0	

[a] Average values of the experimental data of **3** that does not crystallize in a trigonal space group.

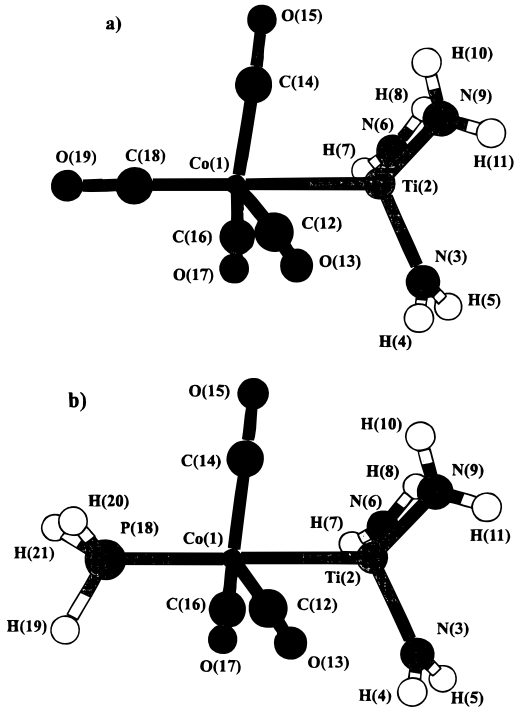

Figure 4. Views of the structures of **3x** (a) and **4x** (b) optimized by DFT (BLYP and B3LYP) methods.

The equatorial CO groups at the cobalt center and the NH_2 groups coordinated to Ti were found to adopt a staggered conformation, as in the experimentally determined structures of **3** and **4b**. The N(3)−Ti(2)−Co(1)−C(12) dihedral angle is about 52°, with a barrier of rotation around the Co−Ti axis of 5.2 kcal/mol in model system **3x** for both density fuctionals. The configuration of the NH_2 groups, is nearly trigonal planar, as observed for most transition metal amides, and the H(5)−N(3)−Ti(2)−Co(1) dihedral angle is ca. 125°. The barrier of simultaneous rotation of all three NH_2 groups around the Ti−N axes in compound **3x** was found to be 13.8 kcal/mol for both density functionals.

Table 2 also contains a comparison of the calculated structural parameters with corresponding (averaged) quantities from the crystallographically determined structures. It should be remembered that the ligand set of the experimental structures is not exactly the same as that used in the calculations. Since, for example, the orientation of the amido groups is essentially dictated by the geometrical constraints imposed by the framework of the tripodal ligand, a comparison between experimental and calculated values of the dihedral angle between the NR_2 planes and the Ti−Co axis is not meaningful. Besides systematical errors in the available density functionals, the difference in the actual ligand sets is certainly one reason for the deviations of up to 0.09 Å (BLYP) and up to 0.06 Å (B3LYP) for the calculated Co−Ti bond distances in comparison with the experiment.

Nonetheless, the theoretical model does reproduce a prominent effect of the replacement of the axial CO group by a PR_3 group quite well: The experimental result for the contraction of the Co−Ti bond upon this substitution is 0.08 Å, while the calculation yields 0.06−0.07 Å. This bond length variation can be understood on the grounds of back-bonding to the axial CO group with a corresponding weakening of the Co−Ti bond. In summary, the inspection of the data presented in Table 2 suggests that the correspondence between experimental and modeled structural data is very satisfactory and that the B3LYP functional yields a somewhat better representation of the experimental values.

Dissociation Energies

A remarkable feature of the Ti−Co heterobimetallics containing a tripodal amido ligand that are discussed in this paper is their stability as compared to those systems first reported by Selegue et al.[1e] as well as the structurally fully characterized compound $[(t\text{BuO})_3\text{Ti}-\text{Co}(\text{CO})_4]$ described by Selent and coworkers.[1g] While the steric shielding of the metal−metal bond by the tripodal ligand system introduced by us is thought to play an important part in the stabilization of the Ti−Co heterobimetallics, it was of interest to investigate whether there is an additional "thermodynamic" contribution due to the enforced coordination geometry of the amido donor functions.

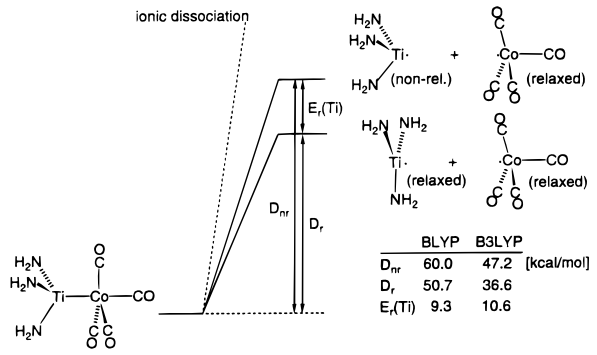

Figure 5. Schematic representation of the energetics associated with the homolytic dissociation of the metal−metal bond in **3x** and **4x**.

We therefore studied the homolytic and heterolytic dissociation of **3x** and **4x**.

In a hypothetical thermodynamic cycle, one can think of the dissociation of the Co−Ti complex as occurring in three steps: First a dissociation into two fragments with the relative arrangement of the ligands fixed in the positions they adopt in the equilibrium structure of the dinuclear complex. The next stage is marked by the relaxation of the ligand positions in one of the two fragments and finally relaxation of the remaining fragment. This experiment is useful in the context of the issue raised above, since the result should give some insight into the importance of the fixed NR_2 ligand positions of the tripod ligand. The Co fragment is not subject to similar geometrical constraints.

Figure 5 schematically represents the overall energetics for the dissociation of **3x** into two neutral fragments. D_r and D_{nr} are the dissociation energies for the dissociation into, respectively, completely relaxed and partially nonrelaxed complex fragments. In the nonrelaxed case, the geometry of the Ti fragment was fixed to that of **3x** while in both cases the Co fragment was energetically minimized (notably, the structural relaxation energy of the Co fragment was rather small: 1.8 and 2.9 kcal/mol for BLYP and B3LYP, respectively). As indicated in Figure 5, the relaxation energy E_r(Ti) of the Ti fragment is about 10 kcal/mol. This represents an upper boundary of the hypothetical relaxation energy of the Ti fragment containing the tripod ligand, which is unable to achieve the planar geometry of the free $Ti(NH_2)_3$ fragment. Therefore, one can estimate that the tripod ligand thermodynamically stabilizes the Co−Ti complex by about 10 kcal/mol.

Unfortunately, the deviation between the dissociation energies obtained using the BLYP and B3LYP functionals are considerable; however, since the three parameters contained in this functional were obtained through a fit to atomization energies, the more realistic value should be the one obtained with the B3LYP functional. It should be noted that this value still needs to be corrected for the zero-point vibration energies to obtain a realistic dissociation energy.

Similar considerations apply to the ionic dissociation of **3x** into a negatively charged Co fragment and a positively charged Ti fragment. The corresponding D_{nr} is about 127.1 and 132.9 kcal/mol in the BLYP and B3LYP cases, respectively, with a relaxation energy of the Ti fragment of about 7.4 and 8.2 kcal/mol.

Finally, we note that substitution of the axial CO group by PH_3 only has a minor influence on the homolytic dissociation energies: D_{nr} for compound **4x** was found to be 58.6 and 45.6 kcal/mol for BLYP and B3LYP functionals, respectively, which marks a slight reduction of about 1.5 kcal/mol as compared to the corresponding value for **3x**.

Population Analysis and Bond Analysis with Natural Atomic Orbitals

Most of the widely used population and bond analysis schemes assign electrons to atoms or pairs of atoms with reference to the atomic basis functions. The simplest procedure is that of Mulliken population analysis (MPA).[27] However, the Natural population analysis (NPA), which is performed in a basis of orthogonal natural atomic orbitals (NAOs),[8,29] is a more refined variant that has proved to be much less sensitive to the quality of the basis set. Table 3 presents NPA-derived partial charges for individual atoms and molecular fragments for our model systems.

The NPA atomic charges obtained by the BLYP and B3LYP functionals are very similar. The most prominent difference is found for the metal centers, for which B3LYP yields a slightly greater (0.1 e) positive charge on the Ti atom and an increased negative charge (also by 0.1 e) on the nearly neutral Co atom. Thus, the difference between the Ti and Co atomic charges is increased from about 1.24 to 1.44 e for **3x** and from 1.29 to 1.50 e for **4x**.[29]

Nevertheless, there is consistency between the charges on the Co and Ti complex fragments calculated with both functionals, the charge difference between the Ti and Co units being 0.70 e for **3x** and only 0.62 e for **4x**. Comparing the charges of **3x** and **4x**, one observes that substitution of the electronically neutral axial CO group by the essentially pure electron donor ligand PH_3 leads to a slight increase in electron density at the Co atom. Concomitant with this change, a slight increase in the group charges on the equatorial CO and the NH_2 ligands is obtained, while the partial charge of the Ti atom remains unaltered.

Table 3 also contains covalent bond orders that were determined from the orthogonal NAO basis according to Wiberg's definition.[9] The metal−ligand bond orders and the bond orders between the ligand atoms are consistent with the intuitive chemical picture: a Ti−N bond order of ca. 1 together with an NH_2 group charge of −0.3 e is about what one would expect for a highly polarized metal−ligand double bond; Co−C bond orders of 0.5−0.7 are reasonable for a dative bond reenforced by metal-to-ligand back-bonding whereas the purely dative Co−P bond is associated with bond orders of only half that magnitude.

The most interesting result listed in Table 3 is the covalent bond order of the metal−metal bond between Co and Ti, which is 0.30 for **3x** and increased by about 0.06 (i.e., 20%) for the axially PH_3-substituted complex **4x**. This result is as intuitively expected and entirely consistent with the notion of the better σ-donor capability of PH_3. The increase in covalent bond order between the metal atoms upon substitution of the axial CO group by PH_3 should, however, not be equated with an increase of the total bond strength. On the contrary, the calculated homolytic dissociation energy decreases slightly (by about 2−3%), which may be interpreted phenomenologically as resulting from a decrease in ionic attraction energy. This is not entirely compensated by the gain in covalent bond energy.

The fairly high complex fragment charges and the low covalent bond orders are not entirely conclusive as to the nature

(27) Mulliken, R. S. *J. Chem. Phys.* **1955**, *23*, 1833, 1841, 2338, 2343.
(28) Reed, A. E.; Weinstock, R. B.; Weinhold, F. *J. Chem. Phys.* **1985**, *83*, 735.
(29) In general, the B3LYP charges suggest a slightly more ionic character of the density. This may be interpreted as being due to the fact that the B3LYP functional contains an intermediate between a pure (gradient corrected) exchange functional and the Hartree−Fock exchange functional; the Hartree−Fock theory being known to yield somewhat too ionic electron densities.

Table 3. Calculated Natural Population Analysis (NPA) Atomic Charges, Molecular Fragment Charges, and Wiberg Bond Orders from Natural Atomic Orbitals for **3x** and **4x**

charges						bond orders					
	3x			**4x**			**3x**			**4x**	
	BLYP	B3LYP		BLYP	B3LYP		BLYP	B3LYP		BLYP	B3LYP
Ti(2)	1.14	1.25	Ti(2)	1.14	1.26	Ti(2)−N(3)	1.10	1.05	Ti(2)−N(3)	1.08	1.03
N(3)	−1.02	−1.07	N(3)	−1.03	−1.07	N(3)−H(4)	0.84	0.84	N(3)−H(4)	0.84	0.84
H(4)	0.37	0.38	H(4)	0.37	0.38	N(3)−H(5)	0.84	0.84	N(3)−H(5)	0.84	0.84
H(5)	0.38	0.39	H(5)	0.38	0.38	Co(1)−Ti(2)	0.30	0.30	Co(1)−Ti(2)	0.37	0.36
NH_2	−0.26	−0.30	NH_2	−0.28	−0.32	Co(1)−C(12)	0.61	0.59	Co(1)−C(12)	0.66	0.63
$Ti(NH_2)_3$	0.35	0.35	$Ti(NH_2)_3$	0.31	0.31	Co(1)−C(18)	0.55	0.52	Co(1)−P(18)	0.26	0.26
Co(1)	−0.10	−0.19	Co(1)	−0.15	−0.24	C(12)−O(13)	2.08	2.07	C(12)−O(13)	2.05	2.05
C(12)	0.37	0.42	C(12)	0.34	0.40	C(18)−O(19)	2.14	2.14	P(18)−H(19)	0.94	0.94
O(13)	−0.45	−0.47	O(13)	−0.46	−0.49						
C(18)	0.42	0.47	P(18)	0.17	0.20						
O(19)	−0.44	−0.46	H(19)	0.01	0.00						
CO_{eq}	−0.08	−0.06	CO	−0.12	−0.09						
CO_{ax}	−0.02	0.01	PH_3	0.20	0.21						
$Co(CO)_4$	−0.35	−0.35	$Co(CO)_3(PH_3)$	−0.31	−0.31						

of the metal−metal bond. One might be led to the conclusion that these bonds are most appropriately described as primarily (or almost purely) ionic. To clarify this point, a charge decomposition analysis (CDA) was carried out[10] starting from the ionic fragments $[Co(CO)_4]^-$ and $[Ti(NH_2)_3]^+$ in which the ligand positions were fixed to those of the complexes.[30] If the metal−metal bond were an essentially ionic bond, it should appear in CDA as a dative bond from $[Co(CO)_4]^-$ to $[Ti(NH_2)_3]^+$, with negligible back-bonding. The CDA analysis performed on **3x** and **4x**, however, yielded a negative back-bonding term of $b = -0.23$ and, more importantly, a nonnegligible residual term ($\Delta = -0.12$ for **3x** and -0.16 for **4x**) due to contributions from virtual orbitals of both fragments. This indicates that an interpretation of the metal−metal bond as a polar covalent bond is more appropriate than an ionic description.[31,32] In contrast, recent CDA investigations of the electronic structure of $[L(CO)_3Co-GaR_2(NH_3)]$ (where L = CO, PH_3 and R = Cl, H) have shown that these compounds indeed can be regarded as $[L(CO)_3Co]-[GaR_2(NH_3)]^+$ donor−acceptor complexes.[21,22]

In summary, the combined results of the NPA partial charge analysis, NAO-based Wiberg bond orders, and CDA support a description of the Ti−Co bonds as highly polarized but nevertheless covalent. Since metal−metal bonds of this type have been barely investigated to date, it was important to verify or falsify this conclusion by means of independent methods that do not rely upon the more or less indirect definitions of atoms and molecular fragments via an orbitalistic approach.

AIM Analysis of the Molecular Charge Distribution

The atoms in molecules theory of Bader[11−13] provides, among many other atomic properties, a definition of atomic charges that is completely different from NPA or any other orbital-based population analysis. Here, atoms are described as open quantum subsystems occupying disjoint regions in real space. The surfaces that separate the atomic domains are constructed from a measurable quantity, the electronic density, by applying the condition that they are crossed nowhere by the gradient field of the electron density distribution ("zero-flux" condition). The advantages of this approach are obvious: First, atomic charges in principle and in practice[33] can be obtained from measured electron densities by integration of the electron density within the atomic domains and adding the nuclear charge. Second, when they are obtained from quantum chemical calculations, they are relatively insensitive to the level of calculation, as is the electron density itself.

The partial atomic and group charges obtained by numerical integration over the atomic domains of **3x** and **4x** are presented in Table 4. By comparing these numbers with the values listed in Table 3, it is apparent that the AIM charges lead to a more polar interpretation of the charge distribution than NPA.[34] For example, the Ti atom now bears a partial charge of nearly two elementary charges, the Co atom becomes positively charged, equatorial CO ligands bear significant negative charges of about −0.3 e, and the charge difference, Δq between C and O atoms amounts to about 2 e. (This number, however, has to be compared to the value of $\Delta q = 2.7$ e obtained in a Bader analysis of the free CO molecule.[11]) Despite this, the overall trends are similar: the B3LYP functional again gives slightly greater partial charges than the BLYP functional, the electron density assigned to the Co atom is increased (i.e., its positive charge reduced) upon substitution with PH_3, while the partial charge of the Ti atom hardly changes and at the same time the partial charges on the fragments are reduced.

Several definitions of bond orders between atoms in molecules have been proposed.[35−37] The definition put forward by Ángyán et al. has a well-defined physical meaning in that it

(30) In CDA, the molecular orbitals of the complex are broken down into contributions from occupied and virtual orbitals of the charged closed-shell fragments.

(31) Frenking, G.; Pidun, U. *J. Chem. Soc., Dalton Trans.* **1997**, 1653.

(32) We would like to point out that CDA performs an analysis of the complex MOs in terms of fragment MOs and that the nonorthogonality of the MOs of *different* fragments may lead to similar difficulties as encountered in MPA, especially when the basis set contains diffuse functions. We have looked into this by carrying out a CDA using a small SVDP basis set described in the calculational section at the end of this paper since this basis set does not contain diffuse d functions in contrast to the TZVDP basis set employed in all our calculations. In this case, the negative back-bonding term is indeed smaller ($b \approx 0.1$); however, the residual term Δ is even larger (between -0.17 and -0.23 depending on the compound and the density functional employed).

(33) Coppens, P. *X-ray Charge Density and Chemical Bonding*; Oxford University Press: Oxford, 1997.

(34) Based on similar observations, it was argued that AIM populations suffer from an artificial charge transfer from an atom with low electronegativity to an adjacent atom with large electronegativity, which was claimed solely to be the consequence of atomic orbital size and not due to differences in electronegativity: Perrin, C. L. *J. Am. Chem. Soc.* **1991**, *113*, 2865. It has been demonstrated, however, that the above argument relies on an oversimplified model and that AIM populations do not depend on atomic size: Gatti, C.; Fantucci, P. *J. Phys. Chem.* **1993**, *97*, 11677.

(35) Cioslowski, J.; Mixon, S. T. *J. Am. Chem. Soc.* **1991**, *113*, 4142.

(36) (a) Fulton, R. L. *J. Phys. Chem.* **1993**, *97*, 7516. (b) Fulton, R. L.; Mixon, S. T. *J. Phys. Chem.* **1993**, *97*, 7530.

(37) Ángyán, J. G.; Loos, M.; Mayer, I. *J. Phys. Chem.* **1994**, *98*, 5244.

Table 4. Calculated Atomic Charges, Molecular Fragment Charges, and Bond Orders Based on AIM for **3x** and **4x**

charges					bond orders				
	3x			**4x**		**3x**			**4x**
	BLYP	B3LYP		BLYP	B3LYP	BLYP	B3LYP		BLYP	B3LYP
Ti(2)	1.88	1.99	Ti(2)	1.88	1.99	Ti(2)−N(3)	0.97	0.93	Ti(2)−N(3)	0.95	0.91
N(3)	−1.15	−1.22	N(3)	−1.15	−1.22	N(3)−H(4)	0.86	0.85	N(3)−H(4)	0.87	0.86
H(4)	0.36	0.37	H(4)	0.35	0.37	N(3)−H(5)	0.86	0.85	N(3)−H(5)	0.87	0.86
H(5)	0.36	0.38	H(5)	0.36	0.37	Co(1)−Ti(2)	0.41	0.42	Co(1)−Ti(2)	0.48	0.48
NH_2	−0.43	−0.46	NH2	−0.44	−0.48	Co(1)−C(12)	1.16	1.15	Co(1)−C(12)	1.21	1.20
$Ti(NH_2)_3$	0.60	0.60	$Ti(NH_2)_3$	0.55	0.56	Co(1)−C(18)	1.04	1.03	Co(1)−P(18)	0.74	0.76
Co(1)	0.41	0.30	Co(1)	0.30	0.18	C(12)−O(13)	1.64	1.58	C(12)−O(13)	1.62	1.56
C(12)	0.78	0.88	C(12)	0.74	0.84	C(18)−O(19)	1.67	1.61	P(18)−H(19)	0.84	0.82
O(13)	−1.06	−1.14	O(13)	−1.07	−1.15						
C(18)	0.89	0.99	P(18)	1.48	1.62						
O(19)	−1.06	−1.13	H(19)	−0.44	−0.48						
CO_{eq}	−0.28	−0.26	CO	−0.34	−0.31						
CO_{ax}	−0.17	−0.14	PH_3	0.16	0.18						
$Co(CO)_4$	−0.60	−0.60	$Co(CO)_3(PH_3)$	−0.55	−0.56						

describes the reduction of the fluctuations aroung the average electron numbers upon uniting the atomic domains of the two bond partnets in a common domain.[38] With the theoretical analysis presented by Mayer in mind,[39] it is readily appreciated that it also may be regarded as a reformulation of the Wiberg bond index (formulated in terms of orthogonalized atomic orbitals) within the language of disjoint spatial atomic domains. Table 4 presents the bond orders determined on the basis of the definition given in ref 37 for our model systems.

The Ti−N bond order of slightly less than 1 together with the high partial charge on the NH_2 group is consistent with a strongly polarized double bond, as was also deduced from the NPA/Wiberg analysis. The Co−C bond order is slightly greater than 1 while the C−O bond order drops to about 1.6 in agreement with the much more polar description of CO in Bader's AIM theory.[40]

In contrast to the results of the previous section, dative bonds are not characterized by low bond orders in the AIM analysis as is indicated by the Co−P bond order of about 0.75. The lowest bond orders in **3x** and **4x** are again found for the metal−metal bond, the value for Ti−Co being somewhat greater in the phosphine-substituted complex **4x**. This again is consistent with a higher polarity of the metal−metal bond in **3x** as reflected by the partial charges of the complex fragments. The fairly low value of less than 0.5 for the metal−metal bond again raises the question of their appropriate description as either ionic or essentially covalent. An analysis of the bond critical point data, which usually provides a good means deciding this question, does not lead to entirely unambiguous results in the case at hand: the density $\rho(\mathbf{r}_c)$ at the at the bond critical point between the metal atoms is only about 0.047 ± 0.005 au, depending on the molecule and the exchange−correlation potential employed. This is rather typical of closed-shell interactions,[11,13a] while the Laplacian of the density $\Delta\rho(\mathbf{r})$ is close to zero in most part of the region between the metal atoms [$\Delta\rho(\mathbf{r}_c) = 0.039 \pm 0.007$]. A vanishing Laplacian means that there is neither a local charge concentration—as usually found for a covalent bond—nor a local charge depletion, as it is typical for closed-shell interactions. The energy density, on the other hand, is slightly negative, $H(\mathbf{r}_c) = -0.012 \pm 0.001$ au, which usually indicates a covalent bond.[13a] This difficulty in the interpretation along with formal objections that can be raised against the AIM bond order analysis in connection with Kohn−Sham DFT[41] led us to consider a bonding description using the electron localization function (ELF). This has been regarded as the most direct way to analyze chemical bonding in molecules and solids.

Description of the Metal−Metal Bonding by Using the Electron Localization Function

The electron localization function (ELF) was originally introduced within the framework of Hartree−Fock theory by Becke and Edgecombe[14] as a function of the spherically averaged probability of finding an electron with a given spin in the neighborhood of another electron with the same spin, which represents an indirect measure for the location of an electron pair with two electrons of opposite spin. ELF is then constructed in such a way that it assumes values of close to 1 when there is a high probability of finding paired electrons (or single, unpaired electrons), and it assumes values close to zero in those regions of space where no electron pairing occurs. Recent work by Savin et al. allowed the extension of the ELF concept to Kohn−Sham density functional theory.[15,42−46]

In Figure 6, two ELF isosurfaces for compound **4x** are shown. The translucent isosurface corresponds to a relatively low ELF value of 0.42 and envelops the solid isosurface that corresponds to ELF = 0.83. The lower of these values allows the discrimination of the different ligands and the core electron regions around the metal atoms. Furthermore, it shows what has to be interpreted as the Co−Ti bond electron pair, i.e., the

(38) Ángyán, J. G. Personal communication.

(39) Mayer, I. *Int. J. Quantum Chem.* **1986**, *29*, 73.

(40) The Hartree−Fock bond order of an isolated CO molecule is about 1.5 according to ref 37; we calculated B3LYP and BLYP bond orders of 1.87 and 1.81 with our TZVDP basis set.

(41) We would like to point out that the significance of AIM bond orders calculated from DFT orbitals is not completely clear, since their derivation for single determinant wave functions involves the first-order density matrix $\rho(\mathbf{r},\mathbf{r}')$.[36,37] For Hartree−Fock wave functions, this quantity can be readily obtained from the Hartree−Fock orbitals as $\rho(\mathbf{r},\mathbf{r}') = \sum n_i\phi_i(\mathbf{r})\phi_i(\mathbf{r}')$. DFT Kohn−Sham orbitals, however, do not yield the electronic density matrix but instead that of a system of noninteracting quasi-particles. By nature of its construction, the trace of this quasi-particle density matrix is equal to the electron density and thus with the trace of the electronic density matrix, however, in general they will not agree for $\mathbf{r} \neq \mathbf{r}'$. On the other hand, the overall characteristics of Kohn−Sham orbitals are similar to those of Hartree−Fock orbitals, in particular, with regard to their bonding and antibonding properties. This makes it unlikely that bond orders determined from Kohn−Sham orbitals are less meaningful than Hartree−Fock bond orders, an assumption that is implicit in the discussion of bonding presented in the previous section.

(42) Savin, A.; Jepsen, O.; Andersen, O. K.; Flad, J.; Preuss, H.; v. Schnering, H. G. *Angew. Chem., Int. Ed. Engl.* **1992**, *31*, 187.

(43) Silvi, B.; Savin, A. *Nature* **1994**, *371*, 683.

(44) Kohout, M.; Savin, A. *Int. J. Quantum Chem.* **1996**, *60*, 875.

(45) Kohout, M.; Savin, A. *J. Comput. Chem.* **1997**, *18*, 1431.

(46) A modified electron localization function that uses the density alone, i.e., without introduction of Kohn−Sham orbitals, has also been proposed: Gadre, S. R.; Kulkarni, S. A.; Pathak, R. K. *J. Chem. Phys.* **1993**, *98*, 3574.

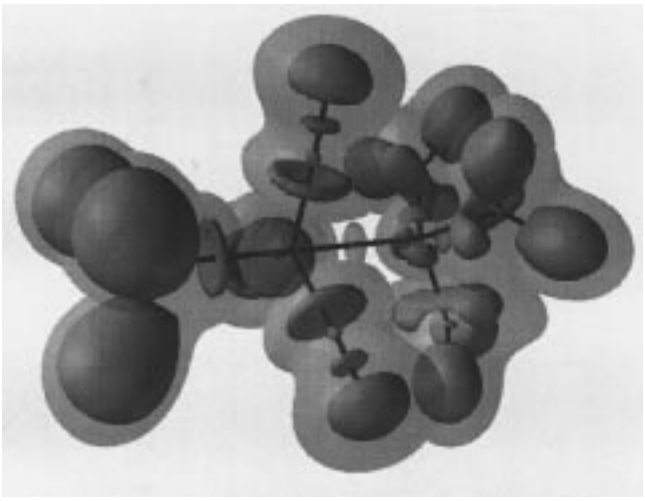

Figure 6. ELF = 0.42 (translucent) and ELF = 0.83 (solid) isosurfaces of **4x** superimposed. The molecule is depicted with the $\{(H_3P)(CO)_3Co\}$ unit at the left-hand side and the $\{Ti(NH_2)_3\}$ unit at the right-hand side of the figure.

small disk around the Co−Ti bond axis approximately in the middle between the metal atoms. The metal−metal bonding electron pair localization isosurface is rather compact, as is also the case for $Re_2(CO)_{10}$,[15] and the ELF maximum within the localization domain is found to be only 0.46. This is rather low as compared to the rule-of-thumb value of about ELF = 0.8 where most covalent bonds, including the Re−Re bond and other homopolar single and multiple metal−metal bonds, are clearly discernible in ELF plots.[15]

We attribute the reason for this unusual bonding representation to a combination of two effects: First, high-angular momentum quantum number orbitals such as d orbitals tend to give rather low contributions to ELF,[45] and a consideration of the frontier orbitals shows that the metal−metal bonding orbital mainly involves the $3d_{z^2}$ orbitals of the metal atoms.[47] Second, and more importantly, the smallness of ELF in the electron localization domain of the metal−metal bond supports its interpretation as a highly polar covalent bond: the bonding electron pair can clearly be identified, but it "dissolves" into a common localization domain with the three isosurfaces encompassing the equatorial carbon monoxide ligands at a slightly lower ELF of 0.40. This situation is comparable to the dissolution of C−F or N−F bonding electron pairs in CF_4 and NF_3 into a common localization domain with the three lone-pair electrons around the fluorine atom.[43,48]

Closer inspection of Figure 6 for the solid ELF = 0.83 surface furthermore reveals the double bonding character of the Ti−N bonds, whose "club-shaped" electron localization domains strongly resemble that found for C−C double bonds,[49] apart from a (not unexpected) strong polarization toward the N atom. The tetrahedral localization domains around the Ti atom represent another interesting feature of the ELF = 0.83 isosurface. They are oriented toward the "holes" between the ligand and Co binding localization domains. Such distortions of the outer core have already been observed in the Laplacian of the electron density of the difluorides and dihydrides of alkali earth metals and can be discussed in similar terms.[50] Finally,

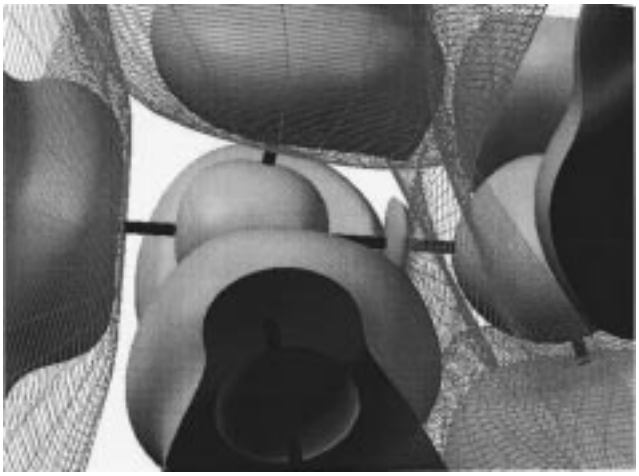

Figure 7. Zoom into the Co−Ti bond region of **4x** for ELF = 0.43, along with some of the Bader atom separating surfaces. The bonding electron pair between the two metal atoms is centered around the Co−Ti bond axis and (at this ELF value) is seen to be localized mainly in the atomic domain of the Co atom.

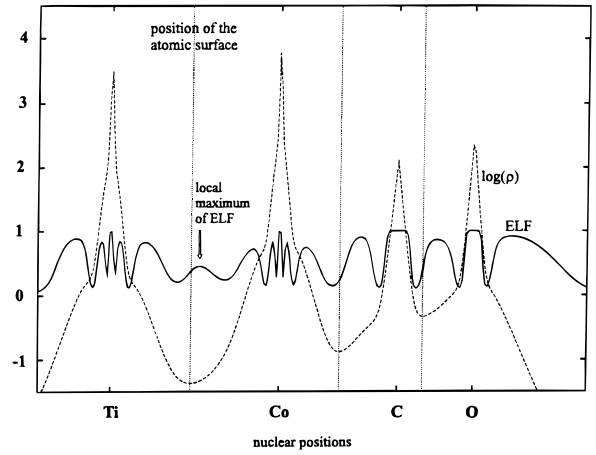

Figure 8. Charge density and ELF profiles of **3**x. The AIM-boundary surfaces, i.e., the corresponding bond critical points, are indicated as dotted lines.

it should be noted that the electron pair localization domains corresponding to the C−O bonds, the N−H and P−H bonds (encompassing, as expected, the hydrogen nuclei), the Co−ligand dative bonds, and the atomic cores can be seen from the ELF = 0.83 isosurface.

Figure 7 shows a superposition of a part of the ELF = 0.43 isosurface with some of the atom-separating surfaces around the metal atoms. Two main observations emerge from this figure: First, all of the ELF isosurfaces around the ligand atoms essentially do not cross the atom-separating surface between the metal atoms and the atom of the ligand closest to it. And second, the metal−metal bond electron pair localization domain being very close to the separating surface between the metal atoms is essentially concentrated on the side of the Co atom. The two observations together suggest that, in the case of heteropolar bonds, ELF is mainly concentrated in the atomic domain of that atom toward which the bond is polarized.

The ELF distribution for compound **3x** shows basically the same features as that for compound **4x**, discussed above. This is delineated by Figure 8 in which ELF and the (logarithmic) electron density profile along the 3-fold symmetry axis of compound **3x** is shown. The position of the bond critical points on this axis is indicated by vertical lines that may be considered as origins of the Bader atom-separating surfaces. This plot

(47) A similar line of reasoning has been used in an ELF analysis of metal−metal bonds in $Rh_6(CO)_{16}$: Kaupp, M. *Chem. Ber.* **1996**, *129*, 527.
(48) Savin, A.; Hässler, T. F. *Chem. Unserer Zeit* **1997**, *31*, 110.
(49) Savin, A.; Silvi, B.; Colonna, F. *Can. J. Chem.* **1996**, *74*, 1088.
(50) (a) Bytheway, I.; Gillespie, R. J.; Tang, T.-H.; Bader, R. W. F. *Inorg. Chem.* **1995**, *34*, 2407. (b) Bader, R. F. W.; Johnson, S.; Tang, T.-H., Popelier, P. L. A. *J. Phys. Chem.* **1996**, *100*, 15398.

clearly indicates the shell structure of ELF for the electron cores of the metal atoms. More importantly, it underlines that the ELF maxima of polar covalent and dative bonds are where one would expect them to be: within the atomic domain of the negatively polarized or donor atom. Thus, combining Bader and ELF analysis leads to a chemically consistent picture of these types of chemical bonds.[51]

Accepting the physically motivated Bader and ELF analysis, which, in contrast to the more traditional means of orbital-based population analysis, can be evaluated more or less directly from a measurable quantity, the electron density, one may ultimately be led to a quantitative theory of our chemically motivated notions of the different bond types. It has been realized that ELF allows a partitioning of three-dimensional space in a very similar way as the electron density itself, via surfaces that fulfill a zero-flux condition and separate electron localization domains, and that integration of the electron density within these domains yields very reasonable values for the average number of electrons concentrated in core and bond domains.[44,49] It has also been noted that dividing the resulting bond populations by a factor 2 leads to a definition of a bond order, which in combination with Bader partial charges of the bonding atoms, provides a qualitative measure of bond polarity: the indicators for a strongly polar covalent bond are a large difference of the partial charges in combination with a low bond population.[15] A strictly quantitative measure might be provided by separate integration of the bond population within each atomic domain of the bond partners. The development of these ideas and their application to a variety of metal−metal bonded complexes is currently under way and will be reported elsewhere.

Conclusions

The quantitative analysis of metal−metal bond polarity in di- or polynuclear complexes reveals the difficulties both of applying the conventional concepts of bond polarity to these systems and of the choice of the quantum chemical electronic structure analysis scheme employed to this end. While molecular orbital-based population analyses may provide a reliable measure of the polarity of a bond, it is only the direct analysis of electron distributions as achieved by the combination of Bader's AIM approach and the recently introduced electron localization function (ELF) that achieves this independent from an MO basis set and enables us to visualize the polarization of the bonding electron pairs in real space. This study presents for the first time a combined approach including these two concepts for the theoretical description of polar metal−metal bonds. The independent methods that were used lead to a consistent picture of the nature of the Ti−Co bonds in the dinuclear complexes prepared by us, which may be summarized as follows:

(1) The covalent metal−metal bond order is less than 0.5 and influenced (b.o. ca. 0.1) by the nature of the trans-axial ligand coordinated to cobalt;

(2) The high partial charges assigned to the complex fragments of greater than 0.5 e emphasize the highly polar character of the Ti−Co bonds;

(3) An interpretation as simple donor−acceptor bonds comparable to the Co group 13 heterobimetallics is inappropriate as derived from the charge decomposition analysis (CDA) and from ELF; in other words, the Ti−Co bonds in **3x** and **4x** are significantly more covalent in nature.

(51) It should be noted that for homopolar bonds the positions of the bond critical points of AIM theory and of the ELF maxima will agree and that the ELF distribution will be symmetrical around that point.

In addition to the description of bond polarity, a theoretical explanation for the unusual stability of the tripod-stabilized unsupported early−late heterobimetallics is offered. It is not only the "protection" of the metal−metal bond that kinetically stabilizes these complexes but also the destabilization of the potential fragments. The coordination geometry that is enforced by the polydentate ligand at the early transition metal center prevents the geometrical relaxation of the fragments, a process that is associated that a change in energy of ca. 10 kcal/mol. This may be viewed as an additional thermodynamic contribution to the stability of the compounds not only described in this work but including those reported previously.

Calculations

All DFT calculations were carried out using the Gaussian94 program package.[52] Atomic charges were determined with a modified version of the Proaim program[53] and bond orders using a program written by J. Ángyán et al.[37] Frontier orbital images were generated with the gOpenMol software.[54] For the three-dimensional visualization of the atomic surfaces and the electron localization function, a program written by one of the authors[55] was employed that provided an interface to the SciAn visualization software.[56]

Most of the electronic structure calculations were carried out with a spherical Gauss type orbital (GTO) basis set of essentially triple ζ-valence double polarization (TZVDP) quality. For the metal atoms, the basis set was derived from the TZVDP basis set developed by Schäfer et al.[57] by augmenting it with diffuse d functions (exponents 0.055 for Ti and 0.10 for Co). This provides additional flexibility to account for variations in the d orbital occupation number.[58] The basis set for the phosphorus atom is derived from the TZVP basis set developed in Ahlrich's group[57] by decontracting the outermost function of the 2p GTO contraction and splitting the single d polarization function of the original basis set into two (exponents 1.0 and 0.3). For all other atoms, the use of two polarization functions was deemed unnecessary; therefore, the unmodified TZVP basis sets of Schäfer et al. was adopted for the H, C, N, and O atoms. The TZVDP basis set comprises 327 and 337 contracted GTOs for the two model systems, respectively.

A smaller basis set of approximately split valence double polarization (SVDP) quality was employed in a series of preliminary structure optimizations. It consists of the SVDP basis set published by Schäfer et al. for the metal atoms,[59] however, with a decontracted outermost d function and the unmodified SVP basis sets of the same reference for all other atoms. Using this smaller basis set, geometry optimizations of the model systems without any symmetry constraints were carried out first, starting from approximate experimental geometries. Not unexpectedly, the resulting structures display nearly perfect C_3 symmetry, apart from slight deviations from the mean values of 0.0002 Å for symmetry-related bond lengths and 0.2 for bond angles. These deviations represent estimates of the numerical accuracy with which the metric parameters were calculated. For the geometry optimizations with the larger basis set, C_3 symmetry constraints have been applied.

(52) Frisch, M. J.; Trucks, G. W.; Schlegel, H. B.; Gill, P. M. W.; Johnson, B. G.; Robb, M. A.; Cheeseman, J. R.; Keith, T.; Petersson, G. A.; Montgomery, J. A.; Raghavachari, K.; Al-Laham, M. A.; Zakrzewski, V. G.; Ortiz, J. V.; Foresman, J. B.; Cioslowski, J.; Stefanov, B. B.; Nanayakkara, A.; Challacombe, M.; Peng, C. Y.; Ayala, P. Y.; Chen, W.; Wong, M. W.; Andres, J. L.; Replogle, E. S.; Gomperts, R.; Martin, R. L.; Fox, D. J.; Binkley, J. S.; Defrees, D. J.; Baker, J.; Stewart, J. P.; Head-Gordon, M.; Gonzalez, C.; Pople, J. A. *Gaussian* 94, Revision D.4; (Gaussian, Inc.: Pittsburgh, PA, 1995).

(53) Biegler-König, F. W.; Bader, R. F. W.; Tang, T. H. *J. Comput. Chem.* **1982**, *3*, 317.

(54) Laaksonen, L. *gOpenMol*; Center for Scientific Computing: Espoo, Finland, 1997.

(55) Jansen, G. Unpublished results.

(56) Pepke, E.; Murray, J.; Lyons, J.; Hwu, T.-Z. *SciAn*; Supercomputer Computations Research Institute, Florida State University: Tallahassee, 1993.

(57) Schäfer, A.; Huber, C.; Ahlrichs, R. *J. Chem. Phys.* **1994**, *100*, 5829.

(58) Hay, P. J. *J. Chem. Phys.* **1977**, *66*, 4377.

(59) Schäfer, A.; Horn. H.; Ahlrichs, R. *J. Chem. Phys.* **1992**, *97*, 2571.

Finally, frequency calculations verified that the resulting structures indeed represent a minimum on the potential energy surface. The total energies obtained with the BLYP functional were −2853.951161 hartree for compound **3x** and −3083.731116 hartree for compound **4x**; the corresponding B3LYP energies were −2853.929648 and −3083.734344 hartree, respectively. We would like to point out that the calculated harmonic IR and Raman spectra of **3x** and **4x** do not exhibit an isolated Co−Ti stretching vibration but instead exhibit several modes of low intensity that contain some amount of ν(Ti−Co). This is in accord with our inability to observe a metal−metal stretching mode in the Raman spectra of the heterobimetallic complexes reported in this study.[60]

The structures of the dissociated fragments were determined in a similar manner, including a harmonic frequency analysis of the final result, using unrestricted DFT in the case of the neutral fragment radicals. When barriers of rotation were calculated, only the corresponding torsion angle was varied with all other structural parameters fixed to their equilibrium values.

Experimental Section

Preparation of the Heterobimetallic Complexes (General Details). All manipulations were performed under an inert gas atmosphere of dried argon in standard (Schlenk) glassware that was flame dried with a Bunsen burner prior to use. Solvents were dried according to standard procedures and saturated with Ar. The deuterated solvents used for the NMR spectroscopic measurements were degassed by three successive freeze−pump−thaw cycles and dried over 4-Å molecular sieves.

The ^{1}H, ^{13}C, ^{29}Si, and ^{31}P NMR spectra were recorded on a Bruker AC 200 spectrometer equipped with a B-VT-2000 variable temperature unit (at 200.13, 50.32, 39.76, and 81.03 MHz, respectively) with tetramethylsilane and H_3PO_4 (85%, ext.) as references. Infrared spectra were recorded on Perkin-Elmer 1420 and Bruker IRS 25 FT spectrometers.

Elemental analyses were carried out in the microanalytical laboratory of the Chemistry Department at Würzburg. The metal complexes MeSi{$SiMe_2N(4\text{-}CH_3C_6H_4)$}$_3$TiBr and MeSi{$SiMe_2N(4\text{-}CH_3C_6H_4)$}$_3$MCl (M = Zr, Hf) were prepared as reported previously by us.[18] The salts of the transition metal carbonylates Na[$Co(CO)_4$], Na[$Co(CO)_3(PPh_3)$], and Na[$Co(CO)_3(PTol_3)$] (Tol = 4-$CH_3C_6H_4$) were synthesized by literature methods.[61] All other chemicals used as starting materials were obtained commercially and used without further purification.

Synthetic Procedure for the Preparation of the Heterobimetallic Complexes 3−6. To a solid mixture of 0.91 mmol of $MeSiSiMe_2N(4\text{-}CH_3C_6H_4)_3MX$ [MX = TiBr (**1**), ZrCl (**2**)] and 1.19 mmol of Na[$Co(CO)_3R$] (R = CO, PPh_3, $PTol_3$) was slowly added 20 mL of cold toluene at −60 °C. The reaction mixture was warmed to room temperature over a period of 10 h and stirred for another 24 h at 30 °C. After evaporating of the solvent, extraction of the residue with 30 mL of pentane, and filtration through a G3-frit, the solution obtained was concentrated to ca. 5 mL. Storage at −30 °C yielded in the heterobimetallic complexes as microcristalline solids.

Analytical and spectroscopic data are as follows:

MeSi{$SiMe_2N(4\text{-}CH_3C_6H_4)$}$_3$Ti−Co(CO)$_4$ (3). Yield: 73%.^{1}H NMR (C_6D_6, 295 K): δ = 0.08 (s, 3 H, CH_3Si), 0.47 (s, 18 H, Si(CH_3)$_2$), 2.12 (s, 9 H, CH_3C$_6$H$_4$), 7.18 (d, 6 H, $^3J(^1H-^1H)$ = 8.7 Hz, H^3), 7.45 (d, 6 H, H^2). ^{1}H^{13}C NMR (C_6D_6, 295 K): δ = −13.1 (CH_3-Si), 2.9 (Si(CH_3)$_2$), 20.9 (*C*H_3C$_6$H$_4$), 125.6 (C^2), 130.0 (C^3), 134.1 (C^4), 148.4 (C^1), 203.4 (CO). {^{1}H}^{29}Si NMR (C_6D_6, 295 K): δ = 7.1 (Si(CH_3)$_2$), −80.6 (CH_3Si). IR (C_6H_6): 2990 w cm^{-1}, 2880 w, 2052 s, 2030 m, 2010 m, 1960 s, br, 1510 m, 1480 m,1285 w, 1248 w, 1200 m, 870 s, 845 m, 812 m, 775 m, 705 m. Anal. Calcd. for $C_{32}H_{42}N_3O_4Si_4TiCo$: C, 51.12; H, 5.63; N, 5.59. Found: C, 50.94; H, 5.47; N, 5.43.

MeSi{$SiMe_2N(4\text{-}CH_3C_6H_4)$}$_3$Ti−Co(CO)$_3$(PPh$_3$) (4a). Yield: 42%. ^{1}H NMR (C_6D_6, 295 K) δ = 0.10 (s, CH_3Si), 0.53 (s, Si(CH_3)$_2$), 2.29 (s, CH_3C$_6$H$_4$), 6.92 (m, C_6H_5), 7.19 (d, H$^{2,3}J(^1H-^1H)$ = 8.4 Hz), 7.64 (d, H^3). {^{1}H}^{13}C NMR (C_6D_6, 295 K): δ = −13.6 (CH_3Si), 2.7 (Si-(CH_3)$_2$), 21.1 (CH_3C$_6$H$_4$), 126.5 (C^2), 128.2 (d, $^3J_{P-C}$ = 9.3 Hz, PPh-C^3), 129.4 (C^3),129.6 (d, $^3J_{P-C}$ = 1.9 Hz, PPh-C^4), 132.1 (C^4), 133.5 (d, $^3J_{P-C}$ = 12.0 Hz, PPh-C^2), 134.3 (d, $^3J_{P-C}$ = 40.7 Hz, PPh-C^1), 150.8 (C^1), 205.8 (CO). {^{1}H}^{31}P NMR (C_6D_6, 295 K) δ = 58.0 (PPh_3). IR (KBr): 2950 w cm^{-1}, 1938 s, 1925 s, 1493 m, 1433 w, 1243 w, 1202 m, 1093 w, 876 m, 853 m, 810 m, 694 m. Anal. Calcd. for $C_{49}H_{57}N_3O_3PSi_4TiCo$: C, 59.68; H, 5.83; N, 4.26. Found: C, 59.35; H, 5.62; N, 4.11.

MeSi{$SiMe_2N(4\text{-}CH_3C_6H_4)$}$_3$Ti−Co(CO)$_3$(PTol$_3$) (4b). Yield: 45%. ^{1}H NMR (C_6D_6, 295 K) δ = 0.14 (s, CH_3Si), 0.51 (s, Si(CH_3)$_2$), 2.04 (s, P(4-CH_3C$_6$H$_4$)$_3$), 2.34 (s, CH_3C$_6$H$_4$), 6.88 (m, P(4-CH_3C$_6$*H*$_4$)$_3$), 7.24 (d, H^2, $^3J(^1H-^1H)$ = 8.1 Hz), 7.69 (d, H^3). {^{1}H}^{13}C NMR (C_6D_6, 295 K): δ = −13.6 (*C*H_3Si), 2.7 (Si(*C*H_3)$_2$), 21.1 (*C*H_3C$_6$H$_4$), 21.2 (P(4-*C*H_3C$_6$H$_4$)$_3$), 126.6 (C^2), 128.6 (d, $^3J_{P-C}$ = 35.1 Hz, PTol-C^1), 129.3 (d, $^3J_{P-C}$ = 12.9 Hz, PTol-C^3), 131.1 (C^4),132.0 (C3), 133.5 (d, $^3J_{P-C}$ = 1.9 Hz, PTol-C^2), 139.7 (PTol-C^4), 150.3 (C^1), 204.4 (CO). {^{1}H}^{31}P NMR (C_6D_6, 295 K) δ = 55.0 ($PTol_3$). IR (KBr): 3020 w cm^{-1}, 2960 w, 2920 w, 1925 s, 1595 w, 1493 m, 1202 m, 1092m, 1018 w, 871 m, 850 m, 805 m, 706 w. Anal. Calcd. for $C_{52}H_{63}N_3O_3PSi_4TiCo$: C, 60.74; H, 6.18; N, 4.09. Found: C, 60.42; H, 6.25; N, 4.35.

MeSi{$SiMe_2N(4\text{-}CH_3C_6H_4)$}$_3$Zr−Co(CO)$_4$ (5). Yield: 37%. ^{1}H NMR (C_6D_6, 295 K): δ = 0.20 (s, 3 H, CH_3Si), 0.49 (s, 18 H, Si-(CH_3)$_2$), 2.13 (s, 9 H, CH_3C$_6$H$_4$), 7.17 (d, 6 H, $^3J(^1H-^1H)$ = 7.7 Hz, H^3), 7.33 (d, 6 H, H^2). ^{1}H^{13}C NMR (C_6D_6, 295 K): δ = −14.8 (*C*H_3-Si), 1.9 (Si(*C*H_3)$_2$), 20.9 (*C*H_3C$_6$H$_4$), 127.2 (C^2), 130.5 (C^3), 134.0 (C^4), 143.2 (C^1), 202.6 (CO). {^{1}H}^{29}Si NMR (C_6D_6, 295 K): δ = −0.4 (Si(CH_3)$_2$), −93.7 (CH_3Si). IR (toluene): 2987 w cm^{-1}, 2981 w, 2051 w, 2021 s, 2006 s, 1601 w, 1498 m, 1476 m, 1423 m, 1356 m, 1287 m, 1243 w, 1108 w, 889 s, 828 m, 797 s, 756, 643 m. Anal. Calcd. for $C_{32}H_{42}N_3O_4Si_4ZrCo$: C, 48.33; H, 5.28; N, 5.32. Found: C; 48.42;H, 5.23; N, 5.46.

MeSi{$SiMe_2N(4\text{-}CH_3C_6H_4)$}$_3$Zr−Co(CO)$_3$(PPh$_3$) (6a). Yield: 42%. ^{1}H NMR (C_6D_6, 295 K) δ = 0.19 (s, CH_3Si), 0.50 (s, Si(CH_3)$_2$), 2.25 (s, CH_3C$_6$H$_4$), 6.90 (m, C_6H_5), 7.13 (d, H^2, $^3J(^1H-^1H)$ = 7.6 Hz), 7.43 (d, H^3). {^{1}H}^{13}C NMR (C_6D_6, 295 K): δ = −15.5 (*C*H_3Si), 1.9 (Si-(CH_3)$_2$), 21.2 (*C*H_3C$_6$H$_4$), 127.5 (C^2), 128.3 (d, $^3J_{P-C}$ = 14.6 Hz, PPh-C^3), 129.7 (C^3), 130.1 (PPh-C^4), 132.2 (C^4), 133.5 (d, $^3J_{P-C}$ = 12.3 Hz, PPh-C^2), 135.0 (d, $^3J_{P-C}$ = 40.6 Hz, PPh-C^1), 145.3 (C^1), 204.3 (CO). {^{1}H}^{29}Si NMR (C_6D_6, 295 K): δ = −4.9 (Si(CH_3)$_2$), −99.2 (CH_3Si). {^{1}H}^{31}P NMR (C_6D_6, 295 K) δ = 59.6 (PPh_3). IR (toluene): 2943 w cm^{-1}, 2928 w, 2001 vw, 1938 vs, 1606 m, 1478 m, 1378 m, 1237 s, 1217 s, 1138 s, 1093 m, 1021 s, 971 m, 886 w, 864 s, 802 s, 732 w, 662 w. Anal. Calcd. for $C_{49}H_{57}N_3O_3PSi_4ZrCo$: C, 57.17; H, 5.58; N, 4.08. Found: C, 57.42; H, 5.63; N, 4.12.

MeSi{$SiMe_2N(4\text{-}CH_3C_6H_4)$}$_3$Zr−Co(CO)$_3$(PTol$_3$) (6b). Yield: 39%. ^{1}H NMR (C_6D_6, 295 K) δ = 0.20 (s, CH_3Si), 0.51 (s, Si(CH_3)$_2$), 1.98 (s, P(4-CH_3C$_6$H$_4$)$_3$), 2.29 (s, CH_3C$_6$H$_4$), 6.83 (d, PTol-H^2, $^3J(^1H-^1H)$ = 7.8 Hz), 6.98 (d, PTol-H^3), 7.17 (d, H^2, $^3J(^1H-^1H)$ = 8.1 Hz), 7.43 (d, H^3). {^{1}H}^{13}C NMR (C_6D_6, 295 K): δ = −15.6 (*C*H_3Si), 1.9 (Si-(*C*H_3)$_2$), 21.1 (*C*H_3C$_6$H$_4$, P(4-*C*H_3C$_6$H$_4$)$_3$), 127.5 (C^2), 129.1 (d, $^3J_{P-C}$ = 10.5 Hz, PTol-C^3), 129.7 (C^3), 132.1 (C^4), 132.2 (d, $^3J_{P-C}$ = 42.5 Hz, PTol-C^1), 133.6 (d, $^3J_{P-C}$ = 12.4 Hz, PTol-C^2), 139.7 (d, $^3J_{P-C}$ = 1.4 Hz, PTol-C^4), 145.5 (C^1), 204.4 (CO). {^{1}H}^{31}P NMR (C_6D_6, 295 K) δ = 56.5 ($PTol_3$). IR (toluene): 2941 w cm^{-1}, 2924 w, 2004 vw, 1933 vs, 1606 m, 1473 m, 1373 m, 1246 s, 1212 s, 1187 w, 1142 s, 1091 m, 1017 s, 964 w, 895 w, 861 s, 832 w, 801 w, 754 w, 684 w, 631 w. Anal. Calcd. for $C_{52}H_{63}N_3O_3PSi_4TiCo$: C, 58.29; H, 5.93; N, 3.92. Found: C, 58.41; H, 5.99; N, 4.01.

X-ray Crystallographic Study of 3, 4b, 5, and 6a. X-ray diffraction data were collected from yellow crystals of **3**, **4b**, **5**, and **6a** mounted in Lindemann tubes under Ar with either a Philips PW1100 or a Siemens P4 four-circle diffractometer using graphite monochromated Mo−Kα radiation. Crystal data and experimental and refinement details are summarized in Table 5.

MeSi{$SiMe_2N(4\text{-}CH_3C_6H_4)$}$_3$Ti−Co(CO)$_4$ (3). A total of 15 124 data were collected in the θ-range 1.62−25.00° with a Siemens P4 diffractometer. The structure wa solved by direct methods, and the remaining non-hydrogen atoms were located from a series of difference Fourier syntheses. The structure was refined on F^2 for 6856 unique data corrected for absorption using a semiempirical method based on

(60) Schätzlein, A.; Schubart, M.; Findeis, B.; Gade, L. H.; Fickert, C.; Pikl, R.; Kiefer, W. *J. Mol. Struct.* **1997**, *408/409*, 373.

(61) (a) Manning, A. R. *J. Chem. Soc. A* **1968**, 1135. (b) Seyferth, D.; Millar, M. D. *J. Organomet. Chem.* **1972**, *38*, 373.

Table 5. Crystal and Refinement Data for Compounds **3**, **4b**, **5**, and **6a**

	3	**4b** $(C_7H_8)_{0.5}(Et_2O)_{0.5}$	**5**	**6a**
		Crystal Data		
formula	$C_{32}H_{42}CoN_3O_4Si_4Ti$	$C_{57.5}H_{72}CoN_3O_{3.5}Si_4PTi$	$C_{32}H_{42}CoN_3O_4Si_4Zr$	$C_{49}H_{57}CoN_3O_3PSi_4Zr$
formula weight, amu	751.88	1111.38	795.20	1029.46
crystal system	monoclinic	rhombohedral	monclinic	cubic
space group	$P2_1/c$	$R\bar{3}$	$P2_1/n$	$Pa\bar{3}$
a, Å	13.1803(11)	15.525(4)	13.3969(14)	22.013(2)
b, Å	14.4195(14)	15.525(4)	14.552(2)	22.013(2)
c, Å	21.488(2)	43.461(10)	21.408(3)	22.013(2)
α, deg	90	90	90	90
β, deg	107.501(6)	90	108.100(6)	90
γ, deg	90	120	90	90
V, Å^3	3894.8(6)	9071.8	3967.1(8)	10666.3(16)
Z	4	6	4	8
ρ_{calc}, g cm^{-3}	1.282	1.221	1.331	1.282
μ[Mo−Kα], mm^{-1}	0.79	0.54	0.84	0.67
F(000)	1568	3516	1640	4272
cryst dimen, mm	0.54 × 0.36 × 0.32	0.40 × 0.40 × 0.32	0.42 × 0.34 × 0.32	0.57 × 0.49 × 0.40
		Data Collection and Processing		
diffractometer	Siemens P4	Philips PW1100	Siemens P4	Siemens P4
λ[Mo−Kα], Å	0.71073	0.71069	0.71073	0.71073
scan mode	*θ*-2*θ*	*θ*-2*θ*	*θ*-2*θ*	*θ*-2*θ*
θ-range, deg	1.62-25.00	3.00-25.00	1.60-25.00	1.60-24.99
limiting indices	$-1 \le h \le 15$	$-19 \le h \le 19$	$-1 \le h \le 18$	$-1 \le h \le 26$
	$-17 \le k \le 17$	$0 \le k \le 19$	$-1 \le k \le 20$	$-1 \le k \le 26$
	$-25 \le l \le 24$	$0 \le l \le 62$	$-30 \le h \le 29$	$-1 \le l \le 26$
data collected	15124	6354	8617	11022
unique data	6856	3539	6969	3137
R_{int}	0.0700	0.0622	0.0545	0.1058
		Structure Analysis and Refinement		
structure solution	direct methods and difference Fourier syntheses	Patterson and difference Fourier syntheses	direct methods and difference Fourier syntheses	direct methods and difference Fourier syntheses
refinement	full-matrix least-squares on F^2	full-matrix least-squares on *F*	full-matrix least-squares on F^2	full-matrix least-squares on F^2
data/parameters	6850/406	964[a]/129	6866/405	3132/188
GooF on F^2	0.999		0.982	1.049
R_1	0.0500,[b] 0.1268	0.0566[a]	0.0648,[b] 0.1730	0.0560,[b] 0.1302
R_w		0.0527[a]		
wR_2	0.0945,[b] 0.1292		0.0832,[b] 0.1325	0.0847,[b] 0.1085
weighting scheme	$[\sigma^2(F_o^2) + (0.0470P)^2 + 0.1984P]^{-1}$	$[\sigma^2(F_o)]^{-1}$	$[\sigma^2(F_o^2) + (0.0288P)^2]^{-1}$	$[\sigma^2(F_o^2) + (0.0339P)^2]^{-1}$
max, min Δe, e A^{-3}	0.316, −0.223	0.337, −0.266	0.338, −0.454	0.275, −0.363

[a] $I > 3\sigma(I)$. [b] $I > 2\sigma(I)$. [c] $P = (F_o^2 + F_c^2)/3$.

Ψ-scans (T_{max} 0.695, T_{min} 0.563). Hydrogen atoms were included in idealized positions and assigned isotropic displacement parameters such as $U_{iso}(H) = 1.5U_{eq}(C)$ of the parent carbon atoms for methyl carbons and $U_{iso}(H) = 1.2U_{eq}(C)$ for phenyl hydrogens. In the final cycles of full-matrix least-squares refinement, all non-hydrogen atoms were assigned anisotropic displacement parameters and refinement converged (max shift/esd < 0.07) at $R_1 = 0.050$ [$I > 2\sigma(I)$] and $wR_2 = 0.1292$ (all data).

MeSi{SiMe$_2$N(4-CH$_3$C$_6$H$_4$)}$_3$Ti−Co(CO)$_3$(PTol$_3$) (4b). A total of 6354 data were collected in the *θ*-range 3.00−25.00° with a Philips PW1100 diffractometer. The positions of the metal atoms were located from a Patterson synthesis, and the remaining non-hydrogen atoms were located from a series of difference Fourier maps. A difference Fourier synthesis calculated with low angle data (sin *θ* < 0.35) revealed the positions of thre methyl hydrogen atoms, and the remaining H-atoms were included in idealized positions. All hydrogen atoms were assigned fixed isotropic displacement parameters of 0.10 Å^2. An area of extende ectectron density surrounding the three center in the crystal was assigned as severely disordered toluene and diethyl ether solvate molecules each of one-half occupancy. After refinement on *F* with isotropic displacement parameters assigned to all atoms, an empirical absorption correction was applied (T_{max} 1.030, T_{min} 0.654). In the final cycles of full-matrix least-squares refinement, the metal and nitrogen atoms and the non-hydrogen atoms of the carbonyl and methylsilane groups were assigned anisotropic displacement parameters and refinement converged (max shift/esd < 0.07) at $R = 0.057$ and $R_w = 0.053$ for 964 data with $I > 3\sigma(I)$.

MeSi{SiMe$_2$N(4-CH$_3$C$_6$H$_4$)}$_3$Zr−Co(CO)$_4$ (5). A total of 8617 data were collected in the *θ*-range 1.60−25.00° with a Siemens P4 diffractometer. The structure was solved by direct methods, and the remaining non-hydrogen atoms were located from a series of difference Fourier syntheses. The methyl carbon [C(17)] of one tolyl group was disordered over two sites of equal occupancy. All hydrogen atoms were included in idealized positions After refinement on F^2 for 6856 unique data with isotropic displacement parameters assigned to all atoms, an empirical absorption correction was applied (T_{max} 0.939, T_{min} 0.370). In the final cycles of full-matrix least-squares refinement, all full-occupancy non-hydrogen atoms were assigned anisotropic displacement parameters and refinement converged (max shift/esd < 0.02) at $R_1 = 0.065$ [$I > 2\sigma(I)$] and $wR_2 = 0.133$ (all data).

MeSi{SiMe$_2$N(4-CH$_3$C$_6$H$_4$)}$_3$Zr−Co(CO)$_3$(PPh$_3$) (6a). A total of 11 022 data were collected in the *θ*-range 1.60−24.99° with a Siemens P4 diffractometer. The structure was solved by direct methods, and the remaining non-hydrogen atoms were located from a series of difference Fourier syntheses. The structure was refined on F^2 for 3137 unique data corrected for absorption using a semiempirical method based on Ψ-scans (T_{max} 0.467, T_{min} 0.428). Hydrogen atoms were included in idealized positions and assigned isotropic displacement parameters such as $U_{iso}(H) = 1.5U_{eq}(C)$ of the parent carbon atoms for methyl carbons and $U_{iso}(H) = 1.2U_{eq}(C)$ for phenyl hydrogens. In the final cycles of full-matrix least-squares refinement, all non-hydrogen atoms were assigned anisotropic displacement parameters and refinement converged (max shift/esd < 0.01) at $R_1 = 0.056$ [$I > 2\sigma(I)$] and $wR_2 = 0.109$ (all data).

Acknowledgment. We thank the Deutsche Forschungsgemeinschaft, the European Commission (TMR network MECATSYN), the Fonds der Chemischen Industrie, the Engineering and Physical Science Research Council, the Deutscher Akademischer Austauschdienst, and the Britisch Council (ARC program) for support. Dedicated to Professor Lord Lewis, a pioneer in the area of metal−metal bonding, on the occasion of his 70th birthday.

Supporting Information Available: Atomic coordinates, thermal parameters, full listings of bond lengths and angles for compounds **3**, **4b**, **5**, and **6a** (33 pages, print/PDF). An X-ray crystallographic file, in CIF format, is available via the Web only. See any current masthead page for ordering information and Web access instructions.

JA974160V